

Wavefunction frozen-density embedding with one-dimensional periodicity: Electronic polarization effects from local perturbations

Cite as: J. Chem. Phys. **157**, 134109 (2022); <https://doi.org/10.1063/5.0102267>

Submitted: 13 April 2022 • Accepted: 30 August 2022 • Accepted Manuscript Online: 31 August 2022 • Published Online: 07 October 2022

 Martha Tordis Wachter-Lehn, Karin Fink and  Sebastian Höfener



View Online



Export Citation



CrossMark

ARTICLES YOU MAY BE INTERESTED IN

[Subsystem density-functional theory: A reliable tool for spin-density based properties](#)

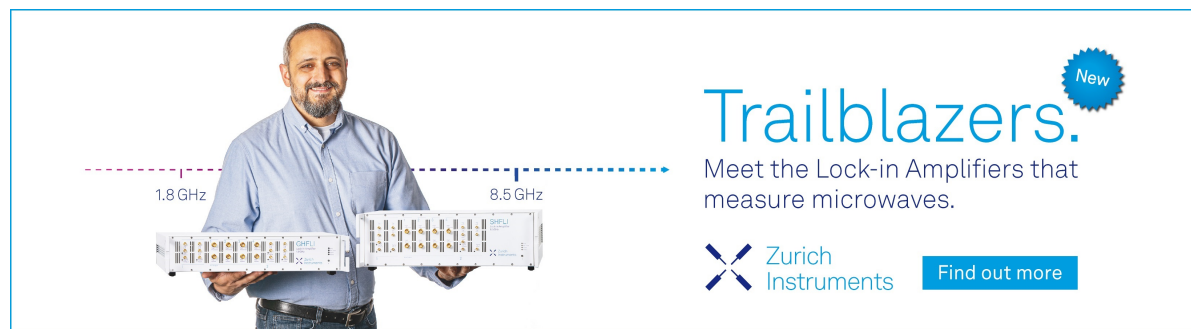
The Journal of Chemical Physics **157**, 130902 (2022); <https://doi.org/10.1063/5.0103091>


[Magnetic-translational sum rule and approximate models of the molecular Berry curvature](#)

The Journal of Chemical Physics **157**, 134108 (2022); <https://doi.org/10.1063/5.0112943>


[Extension of selected configuration interaction for transcorrelated methods](#)

The Journal of Chemical Physics **157**, 134107 (2022); <https://doi.org/10.1063/5.0115524>



Trailblazers. 

Meet the Lock-in Amplifiers that measure microwaves.

 Zurich Instruments [Find out more](#)

Wavefunction frozen-density embedding with one-dimensional periodicity: Electronic polarization effects from local perturbations

Cite as: J. Chem. Phys. 157, 134109 (2022); doi: 10.1063/5.0102267

Submitted: 13 April 2022 • Accepted: 30 August 2022 •

Published Online: 7 October 2022



View Online



Export Citation



CrossMark

Martha Tordis Wachter-Lehn,¹  Karin Fink,² and Sebastian Höfener^{1,a)} 

AFFILIATIONS

¹Institute of Physical Chemistry, Karlsruhe Institute of Technology (KIT), P.O. Box 6980, 76049 Karlsruhe, Germany

²Institute of Nanotechnology, Karlsruhe Institute of Technology (KIT), P.O. Box 3630, 76021 Karlsruhe, Germany

^{a)}Author to whom correspondence should be addressed: hoefener@kit.edu

ABSTRACT

We report an approach to treat polarization effects in a one-dimensional (1D) environment using frozen-density embedding (FDE), suitable to compute response to electron loss or attachment as occurring in organic semiconductors during charge migration. The present work provides two key developments: (a) Local perturbations are computed avoiding an infinite repetition thereof and (b) a first-order equation-of-motion ansatz is used to compute polarization effects due to electron loss and attachment, ensuring an efficient calculation by avoiding open-shell calculations. In a first step, an unperturbed 1D molecular chain is equilibrated using FDE by translation of the center molecule. In a subsequent second step, long-range contributions are frozen and a local perturbation is introduced in the center subsystem. Freeze-thaw iterations are used to relax the electronic wavefunction of both the center subsystem and subsystems in an active region around the center subsystem, avoiding the need to translate the perturbation. The proposed scheme proves to be very efficient and allows for the calculation of charged tetraazaperopyrenes in 1D chains. Due to its efficiency, the new method is capable of providing wavefunction-based reference data relevant for electronic couplings in complex environments.

© 2022 Author(s). All article content, except where otherwise noted, is licensed under a Creative Commons Attribution (CC BY) license (<http://creativecommons.org/licenses/by/4.0/>). <https://doi.org/10.1063/5.0102267>

I. INTRODUCTION

The ground state of a periodic system can be described efficiently by methods using periodic boundary conditions. However, this is not the case anymore for local perturbations in such systems, as polarization effects occur in the surrounding of these perturbations. One solution to this problem is to use large supercells such that the interaction between the local perturbation and its image in the next supercell becomes negligible. The treatment of charged defects is only possible with additional technical tricks, e.g., a background charge to make the cell neutral again.

One example of charged defects is the class of organic semiconductors, where a charge is transported anisotropically depending on the relative positions of the interacting molecules and, thus, also the crystal packing.^{1,2} However, charge transport in organic semiconductors is challenging for traditional charge-transport descriptions such as a band description using Bloch states or polaronic band

models, both of which break down at ambient temperatures.³ On the other hand, charge-hopping models separate the time scale of charge transfer and intermolecular motion. For such charge-hopping models, diabatic electronic states were found to be helpful to understand charge transfer using electron coupling matrix elements between the initial and final states, i.e., before and after charge transfer.⁴

In supermolecular calculations, the charge is often delocalized over the whole system (adiabatic state). However, a local charge is stabilized by orbital relaxation or even geometric changes. The diabatic states required for charge-hopping models, however, are not eigenfunctions of the electronic Hamiltonian of the supersystem. Therefore, a mapping between supermolecular adiabatic states and subsystem diabatic states is in many cases not straightforward. Numerous methods have been employed to compute electronic coupling matrix elements for both charge transfer and exciton transfer.^{2,4} On the one hand, there are supermolecular calculations providing the adiabatic states from which the diabatic coupling

elements are extracted, for which the usual quantum chemistry methods including wavefunction methods are available. For the diabatic states, one has to choose not only the electronic structure method but also the method for generation of diabatic states. Several methods have been employed to diabatize the electron-transfer states, e.g., block diagonalization of the adiabatic electronic Hamiltonian,^{5,6} generalized Mulliken–Hush method (GMH),^{7–13} fragment orbitals,^{14–16} projection methods,^{17,18} and constrained density functional theory (CDFT).^{19–22}

An alternative method to effectively yield localized charge and spin states is given by frozen-density embedding (FDE) developed by Wesolowski and Warshel.^{23–26} This method has received attention in the past due to its reduced scaling properties and the hierarchy of approximations offered by different truncation steps. Besides charge-conserving methods,²⁷ FDE was used to model, e.g., charge transfer reactions, diabatic couplings, or hole transfer reactions for which the donor and acceptor molecules were treated in different subsystems describing inter-subsystem charge transfer.^{28–32} Recently, it was shown that both intra- and inter-subsystem CT excitations can be described correctly using projection-based subsystem time-dependent density functional theory (TDDFT), provided that suitable long-range corrected functionals and basis sets of sufficient flexibility are used.³³

While the references pointed out above rely on methods based on DFT, FDE offers the advantage that it allows us to employ wavefunction based methods to provide an accurate description of charge transfer problems. In order to avoid spin contamination and to investigate higher ionic states, wavefunction methods can be combined with response theory or the equation-of-motion (EOM) ansatz for electron loss or electron attachment.^{34–38} Recently, EOM-based methods have been combined with FDE^{39–41} and also with projector-based embedding.^{42–44}

In the present work, we combine the 1D FDE procedure developed recently⁴¹ with explicit perturbations to account for the electronic polarization, e.g., occurring during charge migration in an organic semiconductor while keeping the long-range contributions fixed to the unpolarized equilibration. FDE is used to separate a charged dimer from the remaining chain, while including a dimer in a subsystem provides adiabatic states and their properties, thereby avoiding inter-subsystem charge transfer excitations, i.e., avoiding diabatic states. This hybrid approach relies on efficient wavefunction methods applicable to, e.g., tetraazaperopyrene (TAPP) dimers to avoid the calculation of coupling matrix elements for coupled electronic states in the case of wavefunction methods.⁴⁵

This article is organized as follows. In Sec. II, the proposed scheme is given, consisting of a first step, in which the 1D periodic system is equilibrated, and a second step, in which a local perturbation is introduced without repetition, computed using a first-order approximation. Section IV provides sample applications for selected case studies. In Sec. IV D, the proposed method is employed to compute energy differences of charged states relevant for electronic coupling matrix elements. Finally, the article closes with our conclusions in Sec. V.

II. METHODS

In the present work, local perturbations in 1D chains are treated in two steps. In the first step, the 1D periodic system is equilibrated

without a specific nonperiodic perturbation being present, as presented in Ref. 41 and briefly reviewed in Sec. II A. In the second step, the center subsystem, denoted as subsystem 0 in the present work, is perturbed and the ground-state electron density of a chosen active region of subsystems is allowed to respond to this perturbation using freeze–thaw (FT) iterations, described in Sec. II B. As a key result of the present work, only the response in a local region around the perturbation is required, avoiding the need to translate the perturbation.

A. Equilibration: Unperturbed 1D periodic chain

1. Frozen-density embedding for an infinite chain

In the FDE scheme, the total density resulting from an infinite amount of subsystems can be expressed as follows:⁴¹

$$\rho_{\text{tot}}(\mathbf{r}) = \sum_{k=-\infty}^{+\infty} \rho_k(\mathbf{r}), \quad (1)$$

where k is an integer and the properties of subsystem 0 shall be determined. Similar to finite systems,^{23–26} the total energy E_{tot} in such a case is formally given as the sum of the subsystem energies $E_k[\rho_k]$ and the interaction energy E_{int} ,

$$E_{\text{tot}}[\rho_0, \rho_{+1}, \rho_{-1}, \rho_{+2}, \rho_{-2}, \dots] = \sum_{k=-\infty}^{+\infty} E_k[\rho_k] + E_{\text{int}}[\rho_0, \rho_{+1}, \rho_{-1}, \rho_{+2}, \rho_{-2}, \dots]. \quad (2)$$

It is implied, however, that for infinite systems, such a total energy adds up to minus infinity and is, thus, never computed. The interaction energy is defined as the difference of the superposition of all densities and the individual subsystem contributions,

$$E_{\text{int}}[\rho_0, \rho_{+1}, \rho_{-1}, \rho_{+2}, \rho_{-2}, \dots] = E_{\text{tot}}[\rho_0 + \rho_{+1} + \rho_{-1} + \dots] - \sum_{l=-\infty}^{+\infty} E[\rho_l]. \quad (3)$$

Using density functional theory for the interaction term, the intra-subsystem Coulomb contributions cancel out, leaving only kinetic and exchange–correlation contributions, both of which require explicit functionals in FDE. To emphasize the nonadditive character of the terms depending on explicit functionals, the latter two terms are termed nonadditive contributions. Thus, the interaction energy can be written as

$$E_{\text{int}} = E_{\text{ES}} + E_{\text{xc,T}}^{\text{nadd}}, \quad (4)$$

$$E_{\text{ES}} = \sum_{l \neq k} \int \rho_l(\mathbf{r}) v_k^{\text{nuc}}(\mathbf{r}) d\mathbf{r} + \frac{1}{2} \sum_{l \neq k} \int \frac{\rho_l(\mathbf{r}) \rho_k(\mathbf{r})}{|\mathbf{r} - \mathbf{r}'|} d\mathbf{r} d\mathbf{r}', \quad (5)$$

$$E_{\text{xc,T}}^{\text{nadd}} = E_{\text{xc,T}}[\rho_0 + \rho_{+1} + \rho_{-1} + \dots] - \sum_{l=-\infty}^{+\infty} E_{\text{xc,T}}[\rho_l]. \quad (6)$$

Note that the dependencies of the densities are omitted for clarity. In FDE, the effective embedding potential to be included, e.g., in the self-consistent field (SCF) equations, is given as the functional derivative of the interaction energy, which can be partitioned into an electrostatic (ES) and a nonadditive (nadd) contribution,

$$v^{\text{emb}} = \frac{\delta E_{\text{int}}}{\delta \rho} = \frac{\delta E_{\text{ES}}}{\delta \rho} + \frac{\delta E_{\text{xc,T}}^{\text{nadd}}}{\delta \rho} = v^{\text{ES}} + v_{\text{xc,T}}^{\text{nadd}}. \quad (7)$$

2. Periodic repetition of one subsystem

So far, the equations describe an infinite chain of general subsystems. For a subsystem repeated infinitely in 1D, one can rewrite the total density as

$$\begin{aligned} \rho_{\text{tot}}(\mathbf{r}) &= \rho_0(\mathbf{r}) + \sum_{k \neq 0}^{\pm\infty} \rho_0(\mathbf{r} + k\mathbf{T}) \\ &= \rho_0(\mathbf{r}) + \sum_{k \geq 1}^{\pm\infty} (\rho_0(\mathbf{r} - k\mathbf{T}) + \rho_0(\mathbf{r} + k\mathbf{T})), \end{aligned} \quad (8)$$

where \mathbf{T} is the translation vector from one molecular center to the molecular center of the nearest neighbor. For the construction of the embedding potential of subsystem 0, the electrostatic contributions can be split into a short-range contribution \mathcal{V} and a long-range contribution \mathcal{W} , depending on the (translated) density ρ_0 of the center subsystem,

$$v^{\text{emb}}[\rho_0] = v_{\text{xc,T}}^{\text{nadd}}[\rho_0] + \mathcal{V}^{\text{ES}}[\rho_0] + \mathcal{W}^{\text{ES}}[\rho_0], \quad (9)$$

where

$$\mathcal{V}^{\text{ES}}[\rho_0](\mathbf{r}) = \sum_{0 < |k|}^N \left(- \sum_{C \neq k} \frac{q_C}{|\mathbf{r} - (\mathbf{R}_C^{(0)} + k\mathbf{T})|} + \int d\mathbf{r}' \frac{\rho_0(\mathbf{r}')}{|\mathbf{r} - (\mathbf{r}' + k\mathbf{T})|} \right). \quad (10)$$

Note that N indicates the subsystem defining the border of long range and short range. The matrix representation of the long-range contributions is computed in an approximate scheme as follows:

$$\begin{aligned} \langle \mu | \mathcal{W}^{\text{ES}}[\rho_0] | \nu \rangle &= \sum_{k > N} \sum_{C \neq k} \frac{q_C}{2} \langle \mu | \nu \rangle \left(\frac{1}{|\mathbf{R}_{AC} - k\mathbf{T}|} + \frac{1}{|\mathbf{R}_{AC} + k\mathbf{T}|} \right. \\ &\quad \left. + \frac{1}{|\mathbf{R}_{BC} - k\mathbf{T}|} + \frac{1}{|\mathbf{R}_{BC} + k\mathbf{T}|} \right), \end{aligned} \quad (11)$$

where q_C are the atomic charges obtained from ρ_0 . For details on the computation of short-range and long-range contributions, the reader is referred to a previous work.⁴¹ For the current work, however, it is only important to note that in the 1D equilibration step, all contributions, i.e., $v_{\text{xc,T}}^{\text{nadd}}[\rho_0]$, $\mathcal{V}^{\text{ES}}[\rho_0]$, $\mathcal{W}^{\text{ES}}[\rho_0]$, are updated until convergence is reached, as they depend on the density ρ_0 of the center subsystem 0.

B. Local perturbations: Freeze-thaw iterations

In the present work, local perturbations, such as charges, are included in a second step after having equilibrated the 1D periodic system. This is achieved by introducing the perturbation in subsystem 0 and allowing cells in close proximity to relax their ground-state electron density due to this perturbation using FT cycles in a state-specific manner. The region being allowed to respond to the perturbation is termed as active region in the present work. Long-range contributions collected in \mathcal{W}^{ES} , however, are kept fixed to the values obtained in the 1D periodic equilibration.

In this perturbation-specific approach, the ground-state density of subsystem 0 is replaced with the perturbed density ρ_0 . The total density partitioning in the FDE scheme for the active region with $2N + 1$ subsystems can thus be written as

$$\rho_{\text{tot}}(\mathbf{r}) = \rho_0(\mathbf{r}) + \sum_{|k| > 0}^N \rho_k(\mathbf{r}), \quad (12)$$

and the energy expression becomes

$$E_{\text{tot}} = E[\rho_0] + \sum_{|k| > 0}^N E[\rho_k] + E_{\text{int}}[\rho_{-N}, \dots, \rho_0, \dots, \rho_{+N}]. \quad (13)$$

The dependence on these densities further carries over to the embedding potential,

$$\begin{aligned} v^{\text{emb}}[\rho_{-N}, \dots, \rho_0, \dots, \rho_{+N}] &= v_{\text{xc,T}}^{\text{nadd}}[\rho_{-N}, \dots, \rho_0, \dots, \rho_{+N}] \\ &\quad + \mathcal{V}^{\text{ES}}[\rho_{-N}, \dots, \rho_0, \dots, \rho_{+N}] + \mathcal{W}^{\text{ES}}. \end{aligned} \quad (14)$$

This notation indicates that the long-range contribution \mathcal{W}^{ES} does not depend on the perturbed densities as it is frozen employing the charges obtained in the unperturbed 1D treatment. It should also be pointed out that only the systems $-N + 1, \dots, N - 1$ are updated in the FT scheme, while the densities of systems $\pm N$ are frozen after the 1D treatment, cf. Sec. III A. However, all $2N + 1$ subsystems of the active region as well as the static long-range contributions are used to construct the embedding potential, see Eq. (14), ensuring a smooth transition at the border of the active region to the unperturbed 1D region.

1. Δ approach for electron loss and attachment

Electron loss or electron attachment can be described by removing or adding electrons from a quantum-chemical calculation, also known as the Δ approach.^{46,47} The Δ approach is directly accessible when unrestricted FDE implementations are available.⁴⁸ For example, in the case of self-consistent field (SCF) methods, the density of the center subsystem 0 is computed from the charged unrestricted reference,

$$\rho_0(\mathbf{r}) = \sum_{\mu\nu} (D_{\mu\nu}^{\alpha} + D_{\mu\nu}^{\beta}) \mu(\mathbf{r}) \nu(\mathbf{r}), \quad (15)$$

with \mathbf{D}^{α} , \mathbf{D}^{β} denoting the back-transformed SCF densities,

$$D_{\mu\nu}^{\sigma} = \sum_{pq} C_{\mu p}^{\sigma} D_{pq}^{\sigma} C_{\nu q}^{\sigma}, \quad (16)$$

where \mathbf{C} are the molecular-orbital (MO) coefficients and σ indicates the spin. Equation (15) together with Eq. (14) is used in the present work to compute the polarization of the active region without the approximate approach, to be discussed in the following.

2. EOM scheme employing excited states

The Δ approach as outlined above can lead to spin contamination, and it leads always to increased computational complexity

TABLE I. Density matrices employed for the polarization of the environment in the proposed approximate scheme based on the configuration interaction singles (CIS) orbital-unrelaxed density matrix. Charge 0 corresponds to a charge-conserving excitation and +1 and -1 to electron loss (IP) and electron attachment (EA), respectively. i, j and a, b denote occupied and virtual molecular orbitals, respectively.

Charge	D_{ij}	D_{ab}
+1	$^{[+1]}D_{ij}^{(n)} = -^{[+1]}X_j^{(n)}\ ^{[+1]}X_i^{(n)}$	—
0	$^{[0]}D_{ij}^{(n)} = -\sum_a\ ^{[0]}X_{aj}^{(n)}\ ^{[0]}X_{ai}^{(n)}$	$^{[0]}D_{ab}^{(n)} = +\sum_i\ ^{[0]}X_{ai}^{(n)}\ ^{[0]}X_{bi}^{(n)}$
-1	—	$^{[-1]}D_{ab}^{(n)} = +\ ^{[-1]}X_a^{(n)}\ ^{[-1]}X_b^{(n)}$

when unrestricted determinants are used instead of restricted determinants. These problems can be circumvented using equation-of-motion (EOM) methods as the electron change is treated similarly to charge-conserving excitations using a closed-shell reference determinant. In this approximate treatment, no explicit spin information is contained, but spin polarization was not found to be dominating for polarization of separated molecules.⁴⁸

In general, the perturbed density can be expressed as a sum of ground-state and excited contribution using EOM methods,

$$\rho_0(\mathbf{r}) = \sum_{\mu\nu} \left(D_{\mu\nu}^{\text{SCF}} + ^{[-1/0/+1]}D_{\mu\nu}^{(n)} \right) \mu(\mathbf{r})\nu(\mathbf{r}), \quad (17)$$

where $D_{\mu\nu}^{\text{SCF}}$ and $^{[-1/0/+1]}D_{\mu\nu}^{(n)}$ denote the closed-shell back-transformed SCF and transition densities. The fact that it is often sufficient to treat the inter-subsystem interaction at a reduced complexity when employing FDE⁴⁹ motivates the use of configuration interaction singles (CIS) and Tamm–Dancoff approximation (TDA) schemes to polarize the environment subsystems in the FT scheme. In these methods, excited-state vectors \mathbf{X} are obtained in general from an eigenvalue equation,

$$\mathbf{A}\mathbf{X}^{(n)} = \omega_n\mathbf{X}^{(n)}, \quad (18)$$

where \mathbf{A} is the response matrix and ω the eigenvalue. The index n denotes state-dependent quantities. The response matrices relevant for the polarization of the environment are obtained for closed-shell systems as

$$^{[-1]}A_{a,b} = \varepsilon_a\delta_{ab}, \quad (19)$$

$$^{[0]}A_{ia,jb}^{\text{CIS}} = (\varepsilon_a - \varepsilon_i)\delta_{ij}\delta_{ab} + 2(ia|g_{12}|jb) - (ij|g_{12}|ab), \quad (20)$$

$$^{[0]}A_{ia,jb}^{\text{TDA}} = (\varepsilon_a - \varepsilon_i)\delta_{ij}\delta_{ab} + 2(ia|g_{12}|jb) - (ij|s_{12}|ab) + (ia|w_{xc}|jb), \quad (21)$$

$$^{[+1]}A_{ij} = -\varepsilon_i\delta_{ij}. \quad (22)$$

In this notation, [0] corresponds to a charge-conserving excitation and [+1], [-1] to electron loss and electron attachment, respectively, and ε are the orbital energies. g_{12} is the conventional two-electron Coulomb repulsion operator; furthermore,

$$\langle pr|s_{12}|rs \rangle = \left\langle pr \left| \frac{\alpha + \beta \text{erf}(\eta r_{12})}{|\mathbf{r}_1 - \mathbf{r}_2|} \right| rs \right\rangle. \quad (23)$$

It should be pointed out that the proposed approximate scheme effectively corresponds to removing one occupied orbital or adding one virtual orbital to the ground-state density matrix in the case of electron loss (IP) and electron attachment (EA), respectively, to compute the polarization of the active region. As this treatment is in agreement with adiabatic diagrammatic construction to first order [ADC(1)], the method will be denoted as ADC(1) in the following to highlight the first-order character. However, having solved the target eigenvalue equation, the state-specific density is computed from the solution vector \mathbf{X} according to Table I, to be used in Eq. (17) and eventually in the embedding potential, Eq. (14). The results are compared with the Δ approach, cf. Sec. II B 1.

III. COMPUTATIONAL DETAILS

All methods employed in the present work are available in the KOALA program using git revision bdc46502cd9. Embedding calculations have been carried out employing PBE⁵⁰ as the exchange–correlation functional and PW91k⁵¹ as the kinetic energy functional for the nonadditive contributions unless stated otherwise. Both the embedded 1D periodic and perturbed systems have included effective potentials on all environment atoms.⁵²

Correlated methods used were EOM-IP as well as EOM-EA variants of the second-order algebraic diagrammatic construction scheme [ADC(2)],^{40,53} employing the frozen-core approximation. Uncorrelated methods—i.e., Hartree–Fock, configuration interaction singles (CIS), ground-state density functional theory (DFT), and excited states in the Tamm–Dancoff approximation (TDA)—have been carried out using semi-numeric exchange, cf. the Appendix. If not stated otherwise, the def2-SVP basis was employed.^{54,55} Functionals used were B3LYP,^{56–59} CAMB3LYP,^{60,61} and ω B97.⁶² The ω B97 functional was implemented in a local version of xcfun.⁶³

The geometry of the water chain and the TAPP chains was taken from Ref. 41. Perturbed water chain information and details of the hydrogen chain are provided in the supplementary material.

A. Computational protocol

As outlined above, in the first step, the 1D periodic system is equilibrated without a perturbation beyond the 1D environment being present, cf. Fig. 1. The procedure starts by computing subsystem 0 in vacuum, from which the embedding potential is constructed by translation of the obtained density. Using macroiterations, subsystem 0 is updated in the presence of the embedding

Procedure	Subsystem index											
	...	-N	-N+1	...	-1	0	1	...	N-1	N	...	
Equilibration	1. Initial	0	0	0	0	0	ρ_0^*	0	0	0	0	0
	2. Macroiterations	ρ_0^*	ρ_0^*	ρ_0^*	ρ_0^*	ρ_0^*	ρ_0^*	ρ_0^*	ρ_0^*	ρ_0^*	ρ_0^*	ρ_0^*
	3. Unpolarized env.	ρ_0	ρ_0	ρ_0	ρ_0	ρ_0	ρ_0	ρ_0	ρ_0	ρ_0	ρ_0	ρ_0
Perturbation	1. Initial	ρ_0	ρ_0	ρ_0	ρ_0	ρ_0	ρ_0^*	ρ_0	ρ_0	ρ_0	ρ_0	ρ_0
	2. FT iterations	ρ_0	ρ_0	ρ_{-N+1}^*	...	ρ_{-1}^*	ρ_0^*	ρ_1^*	...	ρ_{N-1}^*	ρ_0	ρ_0
	3. Polarized env.	ρ_0	ρ_0	ρ_{-N+1}	...	ρ_{-1}	ρ_0	ρ_1	...	ρ_{N-1}	ρ_0	ρ_0

FIG. 1. Total scheme including both equilibration of the unperturbed system and perturbation. A star indicates the densities being optimized in each step. For equilibration, first the subsystem is computed in vacuum, followed by macroiterations using the translated density. After the equilibration step, all densities are frozen and properties of subsystem 0 can be computed using the unpolarized densities. For the perturbation step, first the perturbed target subsystem density ρ_0 is computed in the presence of the active region employing the equilibrated density ρ_0 , followed by freeze–thaw iterations for the active region, i.e., to update subsystems $-N + 1$ to $+N - 1$ including the target density ρ_0 . After the polarization step, all densities are frozen and properties of the perturbed subsystem 0 can be computed in the presence of the polarized densities.

potential. The so-obtained density is again translated to construct a new embedding potential, ensuring that all subsystems are identical, to eventually yield full self-consistency for the entire chain. In particular, FT iterations are not required in this unperturbed 1D step, as the entire chain is fully equilibrated when the active subsystem is converged.⁴¹

In the second step, from the entire 1D chain, an active region is defined, consisting of target center subsystem 0 and a given number of environment subsystems to take part in the FT scheme, cf. Fig. 1. Beyond the chosen subsystems, the long-range contributions are included as fixed charges. The subsystems $\pm N$ are included in the construction of the embedding potential but kept frozen at all times, i.e., they are not updated in the polarization treatment. Using these constraints, a usual FT scheme is applied, augmented with the long-range charges. In the present work 3 FT iterations are used if not stated otherwise.

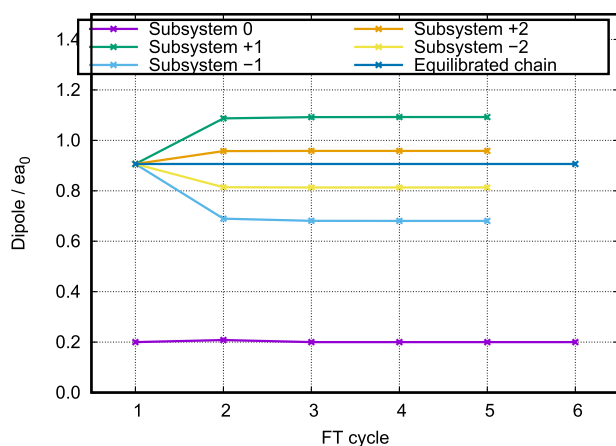


FIG. 2. Convergence of subsystem dipole moments with respect to number of FT cycles for an ionized center water molecule. Interactions are taken into account at the ADC(1) level of theory. The equilibrated 1D chain yields a monomeric dipole moment of $0.906 e a_0$. The monomer in vacuum yields a monomeric dipole moment of $0.802 e a_0$.

In order to illustrate the proposed scheme, in Fig. 2, the convergence with respect to the number of FT cycles is shown for $N = 3$, i.e., a FT scheme consisting of seven water molecules, of which the center water molecule is ionized using the ADC(1) density, cf. Sec. II B. For this example, subsystem 0, i.e., the charged center subsystem, has an almost constant dipole moment of about $0.2 e a_0$ and shows virtually no back polarization. Subsystems ± 1 and ± 2 start in the first FT iteration at the value obtained in the 1D chain and are polarized significantly in the FT scheme due to the newly introduced charge. Subsystems ± 3 remain on the value of the unperturbed chain as they are frozen in the proposed scheme.

In the present work, only total subsystem dipole moments are addressed to estimate the influence of the local perturbation in the target subsystem. Further details could be gained by computing, e.g., effective atomic charges, providing an atomic resolution of the polarization effects. Atomic charges, however, are not uniquely defined and require additional analysis. In the present work, we avoid such discussions and rather investigate the overall strength of the perturbation and its decay with increasing distance from subsystem 0.

IV. RESULTS

In this section, in particular, the accuracy of the spin-free first-order approximate scheme is assessed. It is furthermore addressed how many subsystems must be included to describe the long-range polarization and the behavior of close neighbors in the case of a small active region. We begin by investigating geometry perturbations employing the proposed FT scheme for an active region of the 1D chain in Sec. IV A, for which the ground-state potential can be used. Having established the FT scheme for the active region, state-specific embedding potentials are used to investigate the response of the environment starting in Sec. IV B.

A. Electronic ground state

We start by investigating perturbations in subsystem 0 in the electronic ground state for which the ground-state density is used to construct the embedding potential, equilibrating a 1D water



FIG. 3. View of the manipulated water chain with OH^- and H_3O^+ in the center subsystem 0 in the left and right figure, respectively. In the FT treatment, periodic charges obtained from the 1D FDE approach are also included (not shown in this figure).

chain as described in Sec. II A. In a second step, geometry perturbations are chosen such as rotations and addition and removing protons for a 1D chain of water molecules. Two differently perturbed water chains, i.e., protonated (H_3O^+) and deprotonated (OH^-), are displayed in Fig. 3. Having defined an active region around the perturbation, the electron density of the corresponding molecules are allowed to relax using FT cycles.

In Fig. 4, the ground-state MP2 dipole moment components along the chain are displayed for both H_3O^+ and OH^- for different number of environment subsystems. The notation $1/2N - 2/2$ denotes 1 explicitly perturbed subsystem, surrounded by $2N - 2$ subsystems being allowed to relax to the perturbation, enclosed by 2 subsystems frozen at the state after equilibration of the unperturbed 1D chain, summing in total to an active region consisting of

$2N + 1$ subsystems. The entries “ $1/6/2$ ” thus denote an active region consisting of $2N + 1 = 9$ subsystems, of which 2 are frozen to the 1D equilibration.

Figure 4 reveals a number of features. First, a positive or negative charge leads to a different shift in the dipole moment component along the chain of the water molecules located on the left or right side of the local perturbation. Second, the influence of the charge expands over a long range, as expected for Coulomb charges, and even for $2N + 1 = 33$ molecules, there is a visible difference of the molecules updated (± 15) and the molecules frozen at the equilibrated 1D chain (± 16). Most importantly, however, the figure in particular shows that the closest subsystems, i.e., ± 1 and ± 2 , show only small deviations from a small active region to an increased active region.

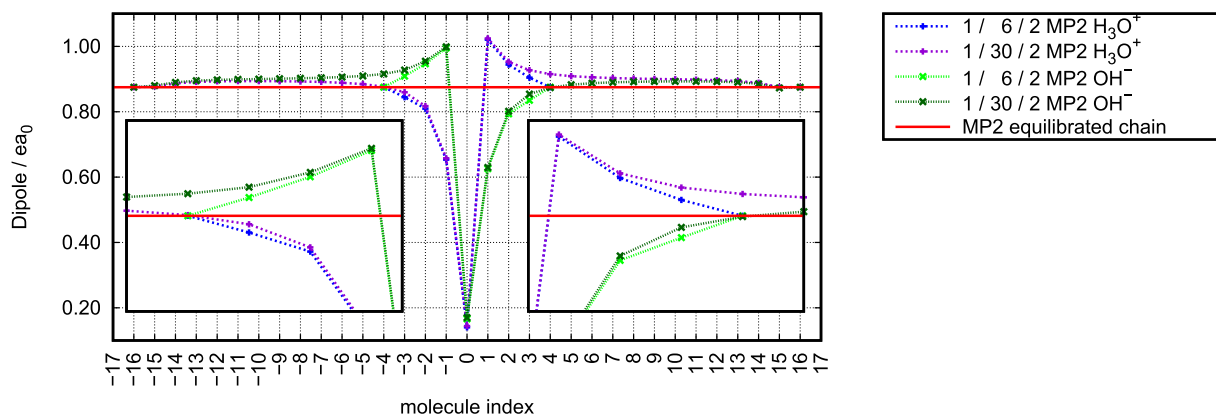


FIG. 4. Convergence of subsystem dipole moments component along the chain with respect to correlation for OH^- vs H_3O^+ .

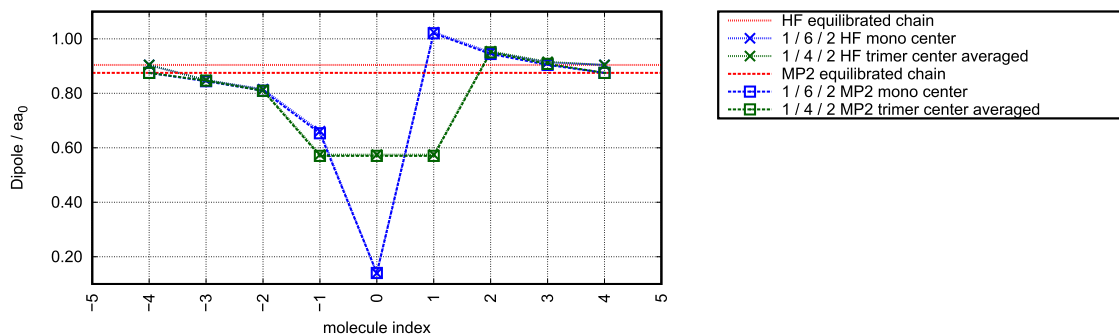


FIG. 5. Dipole moment component along the chain of center subsystem 0 with only H_3O^+ (blue) and $\text{H}_3\text{O}^+ + 2\text{H}_2\text{O}$ (green) molecules in the center subsystem. The blue MP2 curve without averaging corresponds to the one in Fig. 4.

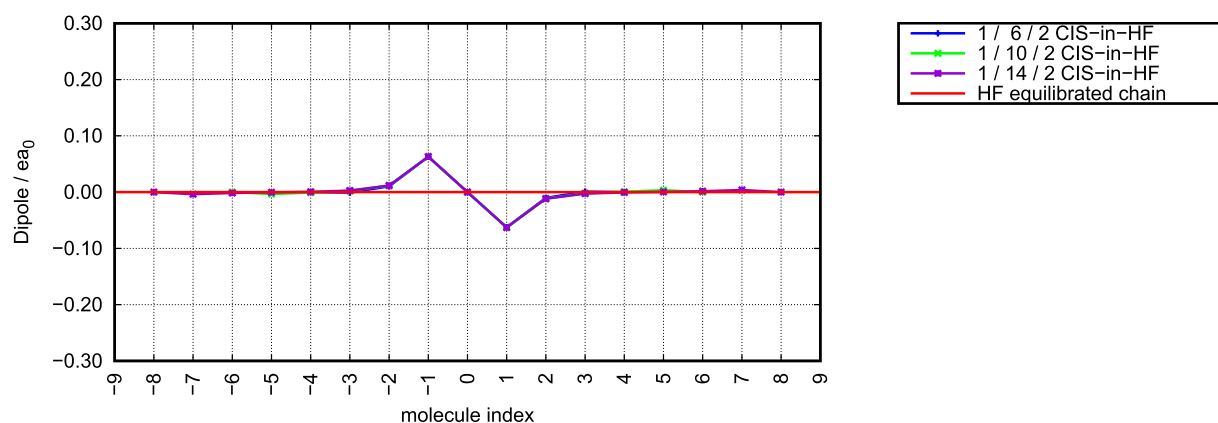


FIG. 6. Convergence of subsystem dipole moment component along the chain with respect to cells (box size 4.0 bohrs) for an excited hydrogen molecule in cell 0 in state S_1 , corresponding to a distance of 4.0 bohrs in Fig. 7.

In Fig. 5, the conceptual analysis and interpretation are illustrated using an H_3O^+ center subsystem 0. Blue curves correspond to one molecule per subsystem, while for the green curves, $H_3O^+ + 2H_2O$ molecules were included in the center subsystem. While in the case of the blue curve, every single molecule has its own response, in the case of three molecules in one subsystem, the average dipole moment ($0.5 a_0$) is obtained by dividing the obtained subsystem dipole moment (about $1.7 a_0$) by the number of molecules. The choice of Hartree-Fock or MP2 does not lead to significant differences in this case as the dipole moment is dominated by the charge. This simple example thus illustrates once more that the average dipole value is not able to provide satisfactory insight into molecular properties, while the subsystem approach offers a conceptual understanding of the influence of local perturbations.

B. Electron-conserving excitations

In Sec. IV A, the proposed two-step approach is illustrated for example, in which the ground-state geometry of subsystem 0 is altered. We now turn to electronic perturbations employing the approximate approach, cf. Sec. II B, leading to state-specific embedding potentials. In the following, the properties of the environment subsystems, e.g., the dipole moment, always refer to their polarized electronic ground state, and the properties of subsystem 0 always refer to the electronically excited state.

In order to analyze the influence of electron-conserving excitations upon the ground-state electron density of the active region, we have chosen the simple case of a chain of hydrogen molecules, see Fig. 6. In this figure, the molecular ground-state dipole moments for the neighbor cells are plotted for an excited hydrogen molecule, with the excited-state dipole moment, located in the center subsystem 0. The figure reveals that the excitation leads only to a short-range polarization in this case. The induced dipole moments have opposite signs as the excitation pushes the electron cloud symmetrically to each side so that molecules to the left and right are polarized in opposite directions.

In Fig. 7, the dipole moment components along the chain are plotted for selected box sizes, corresponding to weaker interactions of the hydrogen molecules for which the bond length 0.75 \AA was fixed. The figure reveals that with increasing box size, the polarization of the environment cells decreases smoothly. The side view (right) in Fig. 7 shows the decrease in the total amount of the induced dipole moment.

C. Electron loss and attachment

Having illustrated the electronic polarization due to excited states with a constant number of electrons, we now turn to the case of electron loss and attachment. The change of electron numbers can either be described by removing or adding electrons in the reference

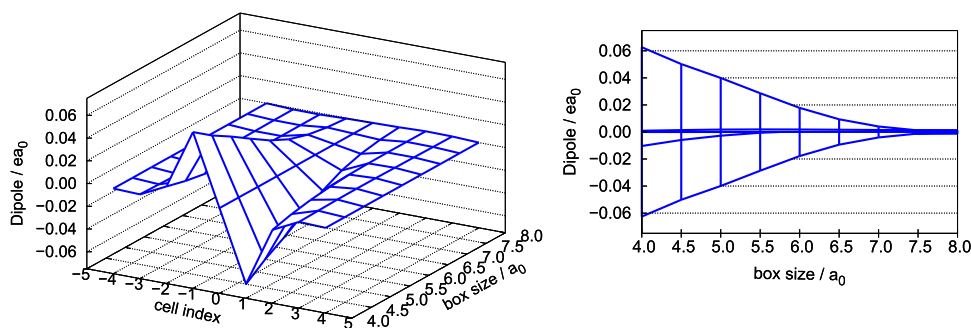


FIG. 7. Convergence of subsystem dipole moment component along the chain with respect to box size for an excited center hydrogen molecule (bond length 0.75 \AA) in state S_1 . Box sizes of 4 and 8 bohrs correspond to intermolecular distances of about 1.37 and 3.48 \AA , respectively. The side view of the 3D plot is given in the right graph, the front view in Fig. 6.

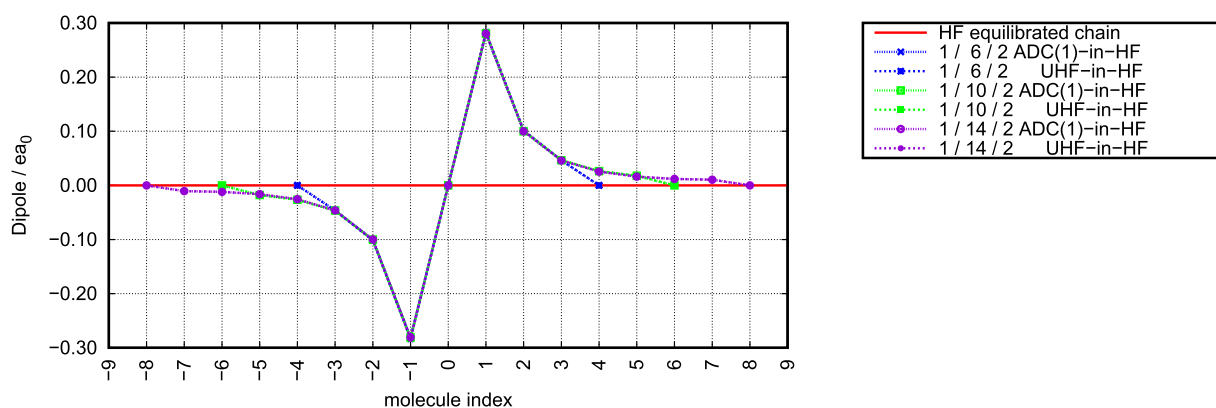


FIG. 8. Convergence of subsystem dipole moment component along the chain with respect to cells (box size 4.0 bohrs) for an ionized hydrogen molecule in cell 0 in the lowest duplet state, D_1 .

determinant or using EOM methods. In the following, these two approaches are compared with respect to different properties using both the water and hydrogen chain as well as a chain H-TAPP-H monomers and *bay*-CF₃-TAPP-H₄Cl₄ dimers.

1. Hydrogen chain

The results for the hydrogen chain are shown in Fig. 8, where one electron has been removed from the center subsystem 0. Compared to the charge-conserving case, the charge introduces a significantly more pronounced electronic polarization in the active region. Due to the electric charge in the center subsystem 0, not only the induced dipole moments increase significantly but also the electronic polarization becomes more long range, extending over several subsystems. Figure 8 reveals that the proposed approximate closed-shell treatment yields only minor deviations with the unrestricted reference case. Remarkably, the first environment cells are obtained accurately even if only three environment cells on each

side are taken into account, independent of the long-range electronic polarization due to the charge. It must be pointed out, however, that in such a comparison, the effect of the active region is analyzed strictly within the uncoupled FDE (FDEu) scheme employed, in which inter-subsystem orbital interactions are not taken into account.

In order to analyze the influence of inter-subsystem orbital interactions, Table II shows the EOM-IP-ADC(2) values in the hydrogen chain example for a small (4.0 a_0) and a large (8.0 a_0) box size for selected active regions and molecules included in subsystem 0. In the case of the 8 a_0 box, the intermolecular electronic coupling is weak, resulting in a red shift of 0.06 eV with respect to the monomer value in the case of supermolecular calculations. The FDEu treatment introduces a small blue shift of 0.03 eV for an active monomer that is compensated when using a pentamer as target subsystem. However, in the case of this box size, no significant inter-subsystem orbital interactions are present and the FDEu scheme does not introduce significant approximations.

TABLE II. EOM-IP-ADC(2) values in eV for selected hydrogen chains consisting of 1, 3, 5, 9, 13, and 17 hydrogen molecules with box sizes of 4.0 and 8.0 a_0 .

Active	4.0 a_0				8.0 a_0			
	Vacuum	9 H ₂	13 H ₂	17 H ₂	Vacuum	9 H ₂	13 H ₂	17 H ₂
Monomer	16.11 ^a	1/6/2 14.12 ^b	1/10/2 14.15 ^b	1/14/2 14.17 ^b	16.11 ^a	1/6/2 16.14 ^b	1/10/2 16.14 ^b	1/14/2 16.14 ^b
Trimer	13.69 ^a	3/4/2 13.11 ^b	3/8/2 13.14 ^b	3/12/2 13.17 ^b	16.05 ^a	3/4/2 16.11 ^b	3/8/2 16.11 ^b	3/12/2 16.11 ^b
Pentamer	12.95 ^a	5/2/2 12.68 ^b	5/6/2 12.71 ^b	5/10/2 12.71 ^b	16.05 ^a	5/2/2 16.08 ^b	5/6/2 16.08 ^b	5/10/2 16.08 ^b
Supermolecule	...	12.46 ^a	12.33 ^a	12.27 ^a	...	16.05 ^a	16.05 ^a	16.05 ^a

^aConventional supermolecular result, with 1, 3, 5, 9, 13, or 17 hydrogen molecules.

^bFDE result, equilibrated in the unperturbed 1D periodic ground state.

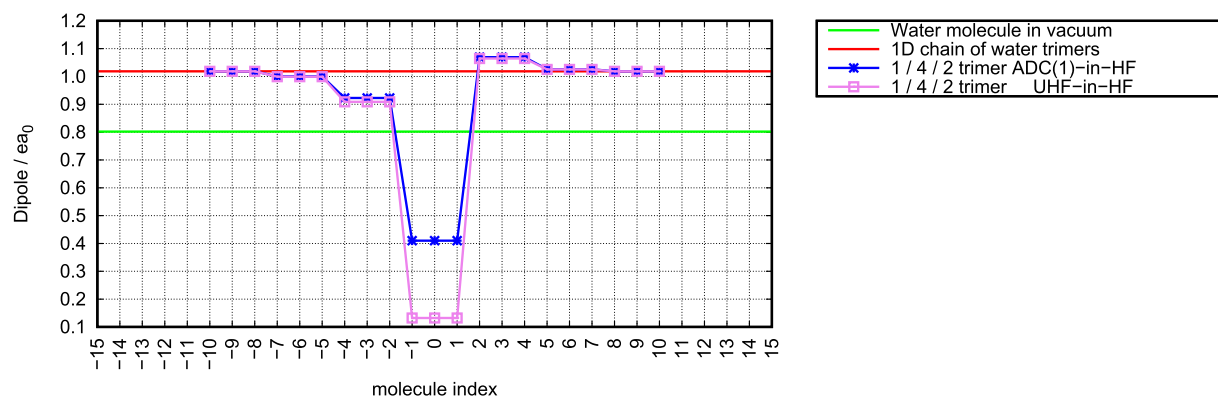


FIG. 9. Convergence of averaged water molecule dipole moments with respect to distance for an ionized center subsystem. All subsystems consist of three water molecules.

In the case of the $4 a_0$ box size, see Table II, the intermolecular electronic coupling is significantly increased, leading to a strongly lowered IP value. The coupling extends over every molecule included in the calculation, leading to a significant shift from 16.11 to 12.95 eV for the IP when going from a monomer to a pentamer, respectively, as well as an additional shift of about -0.68 eV in the case of 17 hydrogen molecules. Note that increasing the system size from 9 H_2 molecules to 17 H_2 still leads to a shift of -0.19 eV in this case. Table II reveals that the embedding treatment leads to an IP of about 14.17 eV if a monomer is used as subsystem 0. This value is about 1.94 eV below the vacuum monomer result, but it still exhibits a significant deviation of about 1.90 eV to the best estimate of 12.27 eV for this box size. Employing a trimer and a pentamer as subsystem 0, the deviation with respect to the best estimate is reduced to ~ 0.90 and 0.44 eV, respectively, revealing on the one hand that there exists a strong influence of the polarized environment and on the other hand that even in the case of the best FDE calculation (12.71 eV), there still exists a non-negligible deviation to the supermolecular calculation. Furthermore, Table II reveals that increasing the active region, however, has only little impact on the IP in this particular example when employing FDEu, even in the case of strongly coupled subsystems.

The reason for the remaining discrepancy of supermolecular and FDEu results in the case of the $4.0 a_0$ box is rooted in the uncoupled FDE (FDEu) approach, in which no orbital information is shared among the subsystems, resulting in a shift that is underestimated with respect to the full supermolecular calculations. For example, in the best FDEu calculation, the orbital interactions of 5 hydrogen molecules (i.e., pentamer) are included, while in the supermolecular calculation, orbital interactions of all 17 hydrogen molecules are taken into account. Orbital interactions can, for example, be included in FDE in the coupled FDE (FDEC) approach,⁶⁴ but such a treatment is beyond the scope of the present work. It must be pointed out, however, that this hydrogen example is an extreme case with an extremely strong coupling in the $4.0 a_0$ box size and a vanishing coupling in the $8.0 a_0$ box size. The other systems investigated in the present work, such as TAPP clusters, can be considered between these two extremes, motivating the use of FDEu, in particular when dimers are used as subsystems.

2. Water chain

Similar to the hydrogen example, one electron can also be removed from center subsystem 0 in the case of the water chain. The electronic polarization of the active region in this case is shown

TABLE III. Induced H-TAPP-H monomer dipole moments due to charge -1 for subsystem 0 ($N = 4$).

PBC ^a	FT ^b	Subsystem							1D ^c
		-3	-2	-1	0	+1	+2	+3	
HF	anion@HF-in-HF	0.208	0.383	0.843	0.000	-0.834	-0.389	-0.270	0.000
	ADC(1)@HF-in-HF	0.216	0.406	0.952	0.000	-0.942	-0.412	-0.277	0.000
B3LYP	anion@B3LYP-in-B3LYP	0.195	0.370	0.814	0.000	-0.807	-0.376	-0.254	0.000
	ADC(1)@B3LYP-in-B3LYP	0.203	0.393	0.929	0.000	-0.920	-0.398	-0.261	0.000
CAMB3LYP	anion@CAMB3LYP-in-CAMB3LYP	0.195	0.368	0.807	0.000	-0.799	-0.373	-0.253	0.000
	ADC(1)@CAMB3LYP-in-CAMB3LYP	0.203	0.392	0.925	0.000	-0.916	-0.397	-0.261	0.000

^aMethod employed in the 1D equilibration.

^bMethods employed in freeze-thaw polarization step.

^cDipole moment in the equilibrated 1D chain.

TABLE IV. Induced H-TAPP-H monomer dipole moments due to charge +1 for subsystem 0 ($N = 4$).

PBC ^a	FT ^b	Subsystem							1D ^c
		-3	-2	-1	0	+1	+2	+3	
HF	cation@HF-in-HF	-0.291	-0.489	-0.756	-0.000	0.753	0.479	0.227	0.000
	ADC(1)@HF-in-HF	-0.299	-0.511	-0.853	0.000	0.848	0.501	0.234	0.000
B3LYP	cation@B3LYP-in-B3LYP	-0.294	-0.478	-0.725	-0.001	0.722	0.469	0.233	0.000
	ADC(1)@B3LYP-in-B3LYP	-0.302	-0.498	-0.820	0.000	0.816	0.489	0.241	0.000
CAMB3LYP	cation@CAMB3LYP-in-CAMB3LYP	-0.290	-0.473	-0.719	-0.001	0.716	0.464	0.229	0.000
	ADC(1)@CAMB3LYP-in-CAMB3LYP	-0.298	-0.494	-0.817	0.000	0.812	0.485	0.237	0.000

^aMethod employed in the 1D equilibration.^bMethods employed in freeze-thaw polarization step.^cDipole moment in the equilibrated 1D chain.

in Fig. 9 when using three water molecules in the center subsystem 0. Note that in this figure, the molecular dipole moments are plotted, which are obtained from averaging the computed dipole moment in the case of subsystem 0. It can be seen that in this case, the approximate approach based on EOM, cf. Sec. II B, differs from the Δ approach serving as a reference. However, it can be seen that the dipole moments differ only for the three molecules contained in the center subsystem 0. Subsystems ± 1 show already only a small deviation, from which it can be concluded that the electronic polarization provided is sufficient to construct the embedding potential. In this case, in the Δ approach, the charge is delocalized over the three water molecules, while in the case of the approximate treatment, the charge seems to be located on one water molecule.

3. TAPP chains

Charged molecules inside complex environments are in particular interesting for organic semiconductors in which a charge is migrating and, thereby, polarizing the neighboring molecules. Results for the H-TAPP-H compound are collected in Tables III and IV for an electron-attached and an electron-detached center subsystem 0, respectively. Dimensions for subsystems and the active region are provided in Table V. In these tables, the subsystems contain only one molecule each. The tables reveal that the spin-free approximate approach based on EOM leads to similar electronic polarization effects compared to the calculations

based on the Δ approach. For this H-TAPP-H compound, the center subsystem dipole moment remains zero, while the molecules to the left and right are polarized with a similar magnitude but in different directions. While the actual numbers differ, the three methods shown, viz., Hartree-Fock, B3LYP, and CAMB3LYP, yield electronic polarization of the subsystems that agrees qualitatively.

Based on the results obtained for H-TAPP-H chain of monomers, we have computed the electronic polarization of the environment cells with the ADC(1) approach for a chain of *bay*-CF₃-TAPP-H₄Cl₄ dimers, displayed in Fig. 10, the results of which are collected in Table VI. In this case, the center subsystem has a nonvanishing dipole moment, which seems to be amplified slightly due to the charge consistently for the HF, B3LYP, and CAMB3LYP methods. In the case of the positive charge, the dipole moment of the center subsystem 0 is even more amplified.

Having investigated the electronic polarization of the environment using the approximate scheme based on EOM, the next step is to investigate the actual properties of the target subsystem 0 using the wavefunction method ADC(2). For example, for a discussion concerning the accuracy of different methods for ionization potentials, see, e.g., Refs. 65 and 66. In Table VII, we have collected the results obtained using different approaches to compute the actual IP and EA values of molecules in a chain. For these calculations, the same dimensions hold as reported in Table V. In this table, the Δ SCF results were computed using the energy of the active subsystem E_I . The results show that in the case of electron loss and electron

TABLE V. Dimensions for the TAPP calculations displayed for each subsystem and an active region with $N = 4$, i.e., 1/6/2. Despite using subsystems, the number of atoms in the active region defines, e.g., the number of ECPs and the integration grid for the entire active region to be included in each subsystem calculation.

System	Subsystem			Active region		
	Molecules	Atoms	Basis ^a	Molecules	Atoms	Basis ^a
H-TAPP-H	1	36	414	9	324	3 726
	2	72	828	18	648	7 452
<i>bay</i> -CF ₃ -TAPP-H ₄ Cl ₄	2	84	1136	18	756	10 224

^adef2-SVP orbital basis.

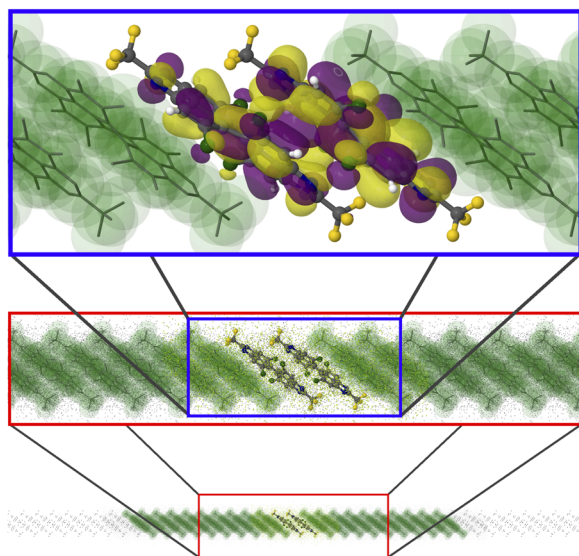


FIG. 10. View of the bay-CF₃-TAPP-H₄Cl₄ chain with effective potentials displayed as transparent green spheres. In the calculation, periodic charges obtained from the 1D FDE approach are also included. Earlier work⁴¹ was carried out without effective potentials.

attachment using EOM methods, a better agreement for the lowest ionic states with the Δ SCF methods B3LYP and CAMB3LYP is obtained when the environment is not polarized.

D. Electronic couplings for molecular charge transfer

Finally, the possibilities offered by the approach proposed in the present work shall be outlined briefly. Using the new method, it becomes possible to compute charge transfer matrix elements inside such a 1D chain for increased system sizes. For symmetric dimers, the diabatic coupling matrix elements $|H_{ab}|$ can be computed from

$$|H_{ab}| = \frac{1}{2} \Delta E, \quad (24)$$

cf. Ref. 67, where ΔE is the energy difference of two adiabatic ionized states. This energy difference can be computed either from the excitation energy $\Delta E = E_1 - E_0$ —where E_1 is the lowest excited cationic state and E_0 is the electronic cationic ground state—in the case of linear-response methods or from $\Delta E = E_2 - E_1$ —where E_2 and E_1 are the second and first excited states, respectively—in the case of EOM methods. Nonsymmetric dimers require using e.g., the GMH method,^{7–13} for which the dipole moments are available in the EOM formalism.⁴⁰

Statistical data of the methods used in the present work with respect to the MRCI+Q method are given in Table VIII. Additional information with respect to the data provided in the table is provided in the supplementary material. A detailed analysis including geometric polarization relevant for reorganization energies, however, is beyond the scope of the present article and will be addressed in a future work. In the present work, we demonstrate the proof of principle that these investigations become possible in the presence of a 1D environment.

Sample results for an ethylene chain consisting of ethylene dimers for hole transfer are collected in Table IX. The table reveals a number of observations. First, the linear-response TDA methods significantly overestimates the coupling for unrestricted reference determinants in the case of the range-separated functionals CAMB3LYP and ω B97. The CIS method, on the other hand, significantly underestimates the coupling by about 200 meV. The table furthermore reveals that the basis set has only a small influence in the case of IP, as the triple-zeta basis shows no qualitative improvement over the split-valence basis. CAS-CI, using an active space of seven electrons in ten spatial orbitals, yields a deviation of about +100 to +150 meV. The DFT results can be improved using orbital-energy differences of the uncharged dimer. It should be highlighted again that in such an EOM approach, the orbitals are not polarized. In the case of the ethylene dimer, the net influence of the 1D environment is found to be rather small for the coupling. However, for example, in the case of CAMB3LYP, each of orbital energies is shifted by about the same amount of 200 meV, resulting in a constant energy difference. The 1D environment thus leads to a non-negligible effect for the individual orbitals but cancels out to a large fraction for relative energies.

Sample results for bay-CF₃-TAPP-H₄Cl₄ for both hole (IP) and electron (EA) transfer are collected in Table X. Analogous

TABLE VI. Induced bay-CF₃-TAPP-H₄Cl₄ dimer dipole moments ($N = 4$), cf. Fig. 10. The 1D equilibration was carried out with the corresponding method (HF, B3LYP, CAMB3LYP).

Charge	FT ^a	Subsystem							1D ^b
		-3	-2	-1	0	+1	+2	+3	
+1	ADC(1)@HF-in-HF	-0.275	-0.673	-2.478	-3.097	1.544	0.427	0.062	-0.592
+1	ADC(1)@B3LYP-in-B3LYP	-0.327	-0.700	-2.550	-2.981	1.649	0.464	0.137	-0.486
+1	ADC(1)@CAMB3LYP-in-CAMB3LYP	-0.315	-0.668	-2.452	-2.944	1.579	0.440	0.127	-0.505
-1	ADC(1)@HF-in-HF	0.255	0.555	1.715	-1.145	-2.211	-0.706	-0.438	-0.592
-1	ADC(1)@B3LYP-in-B3LYP	0.230	0.586	1.819	-1.042	-2.269	-0.722	-0.389	-0.486
-1	ADC(1)@CAMB3LYP-in-CAMB3LYP	0.214	0.557	1.735	-1.043	-2.182	-0.693	-0.373	-0.505

^aMethods employed in freeze-thaw polarization step.

^bDipole moment in the equilibrated 1D chain.

TABLE VII. Vertical IP and EA of H-TAPP-H monomer in eV employing different FT equilibration schemes and methods.

PBC	Pol. ^a	FT equilibration ^b	Method	IP	EA
HF	No	HF-in-HF	LR-ADC(2)	7.296	-1.899
	Yes	HF-in-HF	Δ SCF ^c	5.798 ^d	-1.907
		ADC(1)@HF-in-HF	LR-ADC(2)	6.758	-2.418
B3LYP	No	HF-in-B3LYP	LR-ADC(2)	7.395	-1.998
	Yes	B3LYP-in-B3LYP	Δ SCF ^c	7.519	-1.762
		ADC(1)@HF-in-B3LYP	LR-ADC(2)	6.857	-2.517
CAMB3LYP	No	HF-in-CAMB3LYP	LR-ADC(2)	7.378	-1.981
	Yes	CAMB3LYP-in-CAMB3LYP	Δ SCF ^c	7.760	-1.849
		ADC(1)@HF-in-CAMB3LYP	LR-ADC(2)	6.845	-2.495

^aPolarization of the environment due to charged subsystem 0, cf. Fig. 1.^b $N = 4$.^cComputed from $E_0[\mathcal{Q}_0]$.^d $\langle S^2 \rangle = 2.75$.

to the ethylene dimer, DFT yields rather different results depending on the functional in the case of $\Delta E = E_1 - E_0$, i.e., for the linear-response TDA ansatz using an unrestricted reference. The influence of the basis set, however, is not as significant, as in the case of CAMB3LYP/SVDP, the EA is computed to be 133 meV instead of 135 meV, obtained in the case of CAMB3LYP/SVP. GW@PBE0/def2-TZVP yields 114 meV, see the [supplementary material](#). Using the orbital-energy differences of occupied and

virtual orbitals of the neutral system yields a qualitative agreement with the EOM-IP- and EOM-EA-ADC(2) method, respectively. Altogether, the IP values are significantly altered by the environment, while the EA values remain almost constant. It should be pointed out, however, that the underlying orbitals are shifted by the same amount, leading to a vanishing environment shift. Comparing the energy differences, the tables reveal that EA leads to larger energy differences compared to IP, which might indicate a stronger

TABLE VIII. Statistics of different methods for the calculation of $|H_{ab}|$ in meV, with respect to MRCI+Q.⁶⁷ Further details are given in the [supplementary material](#).

Method	Charge ^a	$2 H_{ab} =$	Basis	MSE ^b	MUE ^c	MRSE/% ^d	MRUE/% ^e	MAX ^f
B3LYP	0	$\epsilon_{\text{HOMO}} - \epsilon_{\text{HOMO}-1}$	SVP	-46.6	46.6	-24.1	24.1	99.7
			TZVP	-39.0	39.0	-17.7	17.7	94.2
CAMB3LYP	0	$\epsilon_{\text{HOMO}} - \epsilon_{\text{HOMO}-1}$	SVP	-26.6	26.6	-15.3	15.3	55.2
			TZVP	-16.5	16.7	-6.4	6.9	44.2
ω B97	0	$\epsilon_{\text{HOMO}} - \epsilon_{\text{HOMO}-1}$	SVP	-61.0	61.0	-31.0	31.0	132.2
			TZVP	-54.9	54.9	-26.3	26.3	127.2
RI-GW@PBE0	0	$\epsilon_{\text{HOMO}} - \epsilon_{\text{HOMO}-1}$	SVP	-44.2	44.2	-23.2	23.2	92.7
			TZVP	-37.6	37.6	-17.9	17.9	87.2
EOM-IP-ADC(2)	0	$E_2 - E_1$	SVP	-15.4	15.6	-9.2	9.3	121.6
			TZVP	-9.0	10.6	-1.9	4.5	112.5
NEVPT2 ^g	+1	$E_1 - E_0$			15.6	-5.8	6.9	50.8
CC2 ^g	+1	$E_1 - E_0$			39.5	+39.8	39.9	72.2

^aCharge of the reference determinant.^bMSE: Mean signed error $\text{MSE} = \frac{1}{n} \sum_n (y_{\text{calc}} - y_{\text{ref}})$.^cMUE: Mean unsigned error $\text{MUE} = \frac{1}{n} \sum_n |y_{\text{calc}} - y_{\text{ref}}|$.^dMRSE: Mean relative signed error $\text{MRSE} = \frac{1}{n} \sum_n (y_{\text{calc}} - y_{\text{ref}}) / y_{\text{ref}}$.^eMRUE: Mean relative unsigned error $\text{MRUE} = \frac{1}{n} \sum_n |y_{\text{calc}} - y_{\text{ref}}| / y_{\text{ref}}$.^fMAX: Maximal unsigned deviation $\text{MAX} = \max |y_{\text{calc}} - y_{\text{ref}}|$.^gReference 67.

TABLE IX. Electronic couplings in meV for the ethylene dimer at a distance of 3.5 Å relevant for hole transport. The reference value for the ethylene dimer using MRCI+Q in vacuum is $|H_{ab}| = 519$ meV.⁶⁷

Basis	$ H_{ab} = \frac{1}{2}(E_1 - E_0)^a$				$ H_{ab} = \frac{1}{2}(E_2 - E_1)^b$				
	TDA-CAMB3LYP	TDA- ω B97	CIS	CAS-CI	B3LYP ^c	CAMB3LYP ^c	EOM-ADC(2)		
Vacuum	def2-SVP	985	659	302	631	420	468	531	×
	def2-TZVPP	955	647	319	678	426	475	507	×
1D chain ^d	def2-SVP	991	663	310	624	425	472	512 ^c	510 ^e
	def2-TZVPP	968	656	333	665	435	485	515 ^c	512 ^e

^aExcitation energy of the first excited state of cation.^bExcitation energy difference of the first and second EOM excited state of neutral dimer.^cNo charge polarization in the ground state.^dPBC: HF; FT equilibration: ADC(1)@HF-in-HF ($N = 4$); method: EOM-ADC(2).^eState-specific approach with charge polarization in the ground state.**TABLE X.** ΔE in meV for the *bay*-CF₃-TAPP-H₄Cl₄ dimer. IP is related to hole transport, EA to electron transport. As the *bay*-CF₃-TAPP-H₄Cl₄ dimer is not symmetric, Eq. (24) cannot be applied to extract the coupling matrix element.⁶⁷

		$\Delta E = E_2 - E_1^a$			$\Delta E = E_1 - E_0^b$	
		B3LYP	CAMB3LYP	EOM-ADC(2)	TDA-CAMB3LYP	TDA- ω B97
Vacuum	IP	50	57	60	76.2	1004.3
	EA	113	135	129	269.3	862.6
1D chain ^c	IP	83 ^d	91 ^d	91 ^e		
	EA	114 ^d	130 ^d	129 ^e		

^aExcitation energy difference of the first and second EOM excited state of neutral dimer.^bExcitation energy of the first excited state of cation.^cPBC: HF; FT equilibration: ADC(1)@HF-in-HF; method: EOM-ADC(2).^dNo charge polarization in the ground state.^eState-specific approach with charge polarization in the ground state.

coupling, which is in agreement with the experimental observation that TAPP compounds are electron transport materials.

As the *bay*-CF₃-TAPP-H₄Cl₄ dimer is not symmetric, Eq. (24) cannot be applied and, thus, there is no one-to-one mapping of the energy difference and the coupling matrix element. Therefore, extensions to Eq. (24) must be investigated,⁶⁷ preventing further conclusions with respect to the charge transfer property of TAPP compounds in the present work. Future work, however, shall be concerned with an in-depth analysis of the energy differences and the extraction of electronic couplings for general, nonsymmetric TAPP compounds. However, the present work is a key step toward this direction, enabling the investigation of TAPP compounds using EOM-ADC(2) methods in 1D chains in future applications.

V. SUMMARY AND CONCLUSIONS

In the present work, we introduce local perturbations in 1D molecular chains using FDE. This is achieved in two decoupled steps. In the first step, an unperturbed 1D molecular chain is equilibrated using FDE to polarize the subsystems with respect to a 1D environment. In the second step, an active region is defined, being allowed to relax the electronic ground-state density with respect to

a geometric or excited-state perturbation in the center subsystem 0. This approach enables treating local defects in otherwise periodic molecular systems without the need to translate the perturbation.

The second main goal of the present work is to establish a first-order approximate computation of electronic polarization effects using restricted wavefunctions to avoid the treatment of unrestricted determinants, which can suffer from spin contamination and increased computational costs. The CIS-based densities, being in agreement with the ADC(1) level of theory, lead to induced dipole moments that are in agreement with the induced dipole moments obtained from unrestricted calculations.

As a third main result, the present work shows that the electronic polarization of the closest neighbor subsystems is not sensitive to the total number of subsystems contained in the active region. This allows for a small active region around the perturbed subsystem 0, rendering the approach particularly efficient.

For symmetric dimers, energy differences of adiabatic states can directly be related to electronic coupling matrix elements for diabatic states relevant to charge transfer. Unfortunately, no simple relation of the adiabatic and diabatic picture is available in the case of nonsymmetric dimers, and the assessment of possible approaches, e.g., such as the generalized Mulliken–Hush method, with respect to TAPP compounds shall be addressed in a future work. However, the

present work provides the properties relevant for such studies using wavefunction methods in complex environments, serving as a key step toward describing charge migration in organic semiconductors using wavefunction-based methods.

SUPPLEMENTARY MATERIAL

See the [supplementary material](#) for more information on molecular geometries, a numerical comparison of the implementation of the semi-numeric exchange, statistics for the accuracy of diabatic couplings H_{ab} , and a selection of vacuum GW results for electronic couplings.

ACKNOWLEDGMENTS

This work was supported by the Deutsche Forschungsgemeinschaft (DFG) through Grant No. SFB 1249 “N-Heteropolycycles as Functional Materials” (Project No. B07).

AUTHOR DECLARATIONS

Conflict of Interest

The authors have no conflicts to disclose.

Author Contributions

Martha Tordis Wachter-Lehn: Investigation (equal). **Karin Fink:** Methodology (equal); Writing – review & editing (equal). **Sebastian Höfener:** Investigation (equal); Methodology (equal); Writing – original draft (lead); Writing – review & editing (equal).

DATA AVAILABILITY

The data that support the findings of this study are available from the corresponding author upon reasonable request.

APPENDIX: SEMI-NUMERIC EXCHANGE

In the semi-numeric approach, the exchange contribution is computed as follows:⁶⁸

$$K_{\mu\nu} = \sum_{\kappa\lambda} (\mu\kappa|s_{12}|\nu\lambda) D_{\kappa\lambda} = \sum_g X_{\mu g} \sum_{\lambda} A_{\nu\lambda}^g F_{\lambda g}, \quad (\text{A1})$$

where

$$X_{\mu g} = \mu(\mathbf{r}_g) \sqrt{w_g}, \quad (\text{A2})$$

$$F_{\lambda g} = \sum_{\kappa} D_{\kappa\nu} X_{\kappa}^g, \quad (\text{A3})$$

$$A_{\nu\lambda}^g = \left(v \left| \frac{\alpha + \beta \operatorname{erf}(\eta r_{12})}{|\mathbf{r} - \mathbf{r}_g|} \right| \lambda \right). \quad (\text{A4})$$

Note that $\alpha = 0.19, \beta = 0.46, \eta = 0.33$ in the case of CAMB3LYP and $\alpha = 0, \beta = 1, \eta = 0.4$ in the case of ω B97. The integral in Eq. (A4) is computed using the Obara–Saika scheme. The nuclear attraction integrals are computed from the basic integrals,

$$\left(\mathbf{0}_A \left| \frac{1}{|\mathbf{r} - \mathbf{C}|} \right| \mathbf{0}_B \right) = 2 \left(\frac{\rho}{\pi} \right)^{1/2} (\mathbf{0}_A | \mathbf{0}_B) F_m(T), \quad (\text{A5})$$

$$\left(\mathbf{0}_A \left| \frac{\operatorname{erf}(\eta r)}{|\mathbf{r} - \mathbf{C}|} \right| \mathbf{0}_B \right) = 2 \left(\frac{\rho}{\pi} \right)^{1/2} (\mathbf{0}_A | \mathbf{0}_B) \sqrt{\frac{\eta^2}{\eta^2 + \rho}} F_m \left(\frac{\eta^2}{\eta^2 + \rho} T \right), \quad (\text{A6})$$

where

$$\rho = \zeta_a + \zeta_b, \quad (\text{A7})$$

$$T = \rho |\mathbf{P} - \mathbf{C}|^2. \quad (\text{A8})$$

Integrals for higher angular momenta are obtained from the usual recursion relations.⁶⁹

REFERENCES

- G. Horowitz, *Adv. Mater.* **10**, 365 (1998).
- V. Coropceanu, J. Cornil, D. A. da Silva Filho, Y. Olivier, R. Silbey, and J.-L. Brédas, *Chem. Rev.* **107**, 926 (2007).
- S. Giannini, A. Carof, M. Ellis, H. Yang, O. G. Ziogos, S. Ghosh, and J. Blumberger, *Nat. Commun.* **10**, 3843 (2019).
- A. Heck, J. J. Kranz, T. Kubař, and M. Elstner, *J. Chem. Theory Comput.* **11**, 5068 (2015).
- T. Pacher, L. S. Cederbaum, and H. Köppel, *J. Chem. Phys.* **89**, 7367 (1988).
- W. Domcke and C. Woywod, *Chem. Phys. Lett.* **216**, 362 (1993).
- R. J. Cave and M. D. Newton, *J. Chem. Phys.* **106**, 9213 (1997).
- R. J. Cave and M. D. Newton, *Chem. Phys. Lett.* **249**, 15 (1996).
- R. S. Mulliken, *J. Am. Chem. Soc.* **74**, 811 (1952).
- N. S. Hush, “Intervalence-transfer absorption. Part 2. Theoretical considerations and spectroscopic data,” *Prog. Inorg. Chem.* **8**, 391–444 (1967).
- N. S. Hush, *Electrochim. Acta* **13**, 1005 (1968).
- J. R. Reimers and N. S. Hush, *J. Phys. Chem.* **95**, 9773 (1991).
- C. Creutz, M. D. Newton, and N. Sutin, *J. Photochem. Photobiol., A* **82**, 47 (1994).
- A. Farazdel, M. Dupuis, E. Clementi, and A. Aviram, *J. Am. Chem. Soc.* **112**, 4206 (1990).
- K. Senthilkumar, F. C. Grozema, F. M. Bickelhaupt, and L. D. A. Siebbeles, *J. Chem. Phys.* **119**, 9809 (2003).
- X. Zeng, X. Hu, and W. Yang, *J. Chem. Theory Comput.* **8**, 4960 (2012).
- A. Migliore, S. Corni, R. Di Felice, and E. Molinari, *J. Chem. Phys.* **124**, 064501 (2006).
- A. Migliore, P. H.-L. Sit, and M. L. Klein, *J. Chem. Theory Comput.* **5**, 307 (2009).
- Q. Wu and T. Van Voorhis, *J. Chem. Phys.* **125**, 164105 (2006).
- Q. Wu and T. Van Voorhis, *J. Chem. Theory Comput.* **2**, 765 (2006).
- H. Oberhofer and J. Blumberger, *J. Chem. Phys.* **131**, 064101 (2009).
- H. Oberhofer and J. Blumberger, *J. Chem. Phys.* **133**, 244105 (2010).
- T. A. Wesolowski and A. Warshel, *J. Phys. Chem.* **97**, 8050 (1993).
- A. Severo Pereira Gomes and C. R. Jacob, *Annu. Rep. Prog. Chem., Sect. C: Phys. Chem.* **108**, 222 (2012).
- C. R. Jacob and J. Neugebauer, *Wiley Interdiscip. Rev.: Comput. Mol. Sci.* **4**, 325 (2014).
- T. A. Wesolowski, S. Shedge, and X. Zhou, *Chem. Rev.* **115**, 5891 (2015).
- S. Höfener, A. Severo Pereira Gomes, and L. Visscher, *J. Chem. Phys.* **136**, 044104 (2012).
- M. Pavanello and J. Neugebauer, *J. Chem. Phys.* **135**, 234103 (2011).
- M. Pavanello, T. Van Voorhis, L. Visscher, and J. Neugebauer, *J. Chem. Phys.* **138**, 054101 (2013).
- P. Ramos, M. Papadakis, and M. Pavanello, *J. Phys. Chem. B* **119**, 7541 (2015).

- ³¹A. Solovyeva, M. Pavanello, and J. Neugebauer, *J. Chem. Phys.* **140**, 164103 (2014).
- ³²D. G. Artiukhin and J. Neugebauer, *J. Chem. Phys.* **148**, 214104 (2018).
- ³³J. Tölle, M. Böckers, N. Niemeyer, and J. Neugebauer, *J. Chem. Phys.* **151**, 174109 (2019).
- ³⁴A. Shee, T. Saue, L. Visscher, and A. Severo Pereira Gomes, *J. Chem. Phys.* **149**, 174113 (2018).
- ³⁵S. Hirata, M. Nooijen, and R. J. Bartlett, *Chem. Phys. Lett.* **328**, 459 (2000).
- ³⁶M. Nooijen and R. J. Bartlett, *J. Chem. Phys.* **102**, 3629 (1995).
- ³⁷M. Musiał, S. A. Kucharski, and R. J. Bartlett, *J. Chem. Phys.* **118**, 1128 (2003).
- ³⁸J. F. Stanton and J. Gauss, *J. Chem. Phys.* **101**, 8938 (1994).
- ³⁹Y. Bouchafra, A. Shee, F. Réal, V. Vallet, and A. Severo Pereira Gomes, *Phys. Rev. Lett.* **121**, 266001 (2018).
- ⁴⁰J. Liu, C. Hättig, and S. Höfener, *J. Chem. Phys.* **152**, 174109 (2020).
- ⁴¹K. Fink and S. Höfener, *J. Chem. Phys.* **154**, 104114 (2021).
- ⁴²T. A. Barnes, J. W. Kaminski, O. Borodin, and T. F. Miller III, *J. Phys. Chem. C* **119**, 3865 (2015).
- ⁴³S. J. Bennie, B. F. E. Curchod, F. R. Manby, and D. R. Glowacki, *J. Phys. Chem. Lett.* **8**, 5559 (2017).
- ⁴⁴X. Wen, D. S. Graham, D. V. Chulhai, and J. D. Goodpaster, *J. Chem. Theory Comput.* **16**, 385 (2020).
- ⁴⁵S. Höfener and L. Visscher, *J. Chem. Theory Comput.* **12**, 549 (2016).
- ⁴⁶R. O. Jones and O. Gunnarsson, *Rev. Mod. Phys.* **61**, 689 (1989).
- ⁴⁷O. Gunnarsson and B. I. Lundqvist, *Phys. Rev. B* **13**, 4274 (1976).
- ⁴⁸N. Schieschke, T. Bodenstein, and S. Höfener, *J. Chem. Phys.* **154**, 084120 (2021).
- ⁴⁹J. Heuser and S. Höfener, *J. Chem. Phys.* **148**, 141101 (2018).
- ⁵⁰J. P. Perdew, K. Burke, and M. Ernzerhof, *Phys. Rev. Lett.* **77**, 3865 (1996).
- ⁵¹A. Lembarki and H. Chermette, *Phys. Rev. A* **50**, 5328 (1994).
- ⁵²R. S. Trefl, C. Hättig, and S. Höfener, *J. Chem. Theory Comput.* **18**, 1737 (2022).
- ⁵³J. Schirmer, *Phys. Rev. A* **26**, 2395 (1982).
- ⁵⁴F. Weigend, F. Furche, and R. Ahlrichs, *J. Chem. Phys.* **119**, 12753 (2003).
- ⁵⁵F. Weigend and R. Ahlrichs, *Phys. Chem. Chem. Phys.* **7**, 3297 (2005).
- ⁵⁶A. D. Becke, *J. Chem. Phys.* **98**, 5648 (1993).
- ⁵⁷C. Lee, W. Yang, and R. G. Parr, *Phys. Rev. B* **37**, 785 (1988).
- ⁵⁸P. J. Stephens, F. J. Devlin, C. F. Chabalowski, and M. J. Frisch, *J. Phys. Chem.* **98**, 11623 (1994).
- ⁵⁹S. H. Vosko, L. Wilk, and M. Nusair, *Can. J. Phys.* **58**, 1200 (1980).
- ⁶⁰T. Yanai, D. P. Tew, and N. C. Handy, *Chem. Phys. Lett.* **393**, 51 (2004).
- ⁶¹M. J. G. Peach, T. Helgaker, P. Salek, T. W. Keal, O. B. Lutnæs, D. J. Tozer, and N. C. Handy, *Phys. Chem. Chem. Phys.* **8**, 558 (2006).
- ⁶²J.-D. Chai and M. Head-Gordon, *J. Chem. Phys.* **128**, 084106 (2008).
- ⁶³U. Ekström, L. Visscher, R. Bast, A. J. Thorvaldsen, and K. Ruud, *J. Chem. Theory Comput.* **6**, 1971 (2010).
- ⁶⁴J. Neugebauer, *J. Chem. Phys.* **126**, 134116 (2007).
- ⁶⁵G. Wälz, D. Usvyat, T. Korona, and M. Schütz, *J. Chem. Phys.* **144**, 084117 (2016).
- ⁶⁶S. McKechnie, G. H. Booth, A. J. Cohen, and J. M. Cole, *J. Chem. Phys.* **142**, 194114 (2015).
- ⁶⁷A. Kubas, F. Hoffmann, A. Heck, H. Oberhofer, M. Elstner, and J. Blumberger, *J. Chem. Phys.* **140**, 104105 (2014).
- ⁶⁸P. Plessow and F. Weigend, *J. Comput. Chem.* **33**, 810 (2012).
- ⁶⁹R. Ahlrichs, *Phys. Chem. Chem. Phys.* **8**, 3072 (2006).